

Sensors for the CDF Run2b Silicon Detector

T. Akimoto¹, M. Aoki¹, P. Azzi², N. Bacchetta², S. Behari³, D. Benjamin⁴, D. Bisello², G. Bolla⁵, P. Booth⁶, D. Bortoletto⁵, A. Burghard⁷, G. Busetto², S. Cabrera⁴, A. Canepa⁵, G. Cardoso⁹, M. Chertok¹⁰, C. I. Ciobanu¹¹, P. Cooke⁶, G. Derylo⁹, I. Fang⁹, E.J. Feng¹², J.P. Fernandez⁵, B. Flaughner⁹, J. Freeman¹², L. Galtieri¹², J. Galyardt¹³, M. Garcia-Sciveres¹², G. Giurciu¹³, I. Gorelov⁷, C. Haber¹², D. Hale¹⁴, K. Hara¹, R. Harr¹⁵, C. Hill¹⁴, M. Hoferkamp⁷, J. Hoff⁹, B. Holbrook¹⁰, S.C. Hong¹⁶, M. Hrycyk⁹, T. H. Hsiung¹¹, J. Incandela¹⁴, E.J. Jeon¹⁶, K.K. Joo¹⁶, T. Junk¹¹, H. Kahkola¹⁷, S. Karjalainen¹⁷, S. Kim¹, K. Kobayashi¹⁸, D.J. Kong¹⁶, B. Krieger¹², M. Kruse⁴, S. Kyre¹⁴, R. Lander¹⁰, T. Landry¹⁰, R. Lauhakangas¹⁹, J. Lee¹⁶, R.-S. Lu²⁰, P.J. Lujan¹², P. Lukens⁹, E. Mandelli¹², C. Manea², P. Maksimovic³, P. Merkel⁹, S.N. Min¹⁶, S. Moccia⁹, Y. Nakamura¹, I. Nakano¹⁸, D. Naoumov⁷, T. Nelson⁹, B. Nord³, J. Novak⁵, T. Okusawa²¹, R. Orava¹⁹, Y. Orlov⁹, K. Osterberg¹⁹, D. Pantano², V. Pavlicek⁹, D. Pellett¹⁰, J. Pursley³, P. Riipinen¹⁹, B. Schuyler³, S. Seidel⁷, A. Shenai⁹, A. Soha¹⁰, D. Stuart¹⁴, R. Tanaka¹⁸, M. Tavi¹⁷, H. Von der Lippe¹², J.-P. Walder¹², Z. Wang², P. Watje⁷, M. Weber¹², W. Wester⁹, K. Yamamoto²¹, Y.C. Yang¹⁶, W. Yao¹², W. Yao¹⁰, R. Yarema⁹, H. Yoshitama¹, J.C. Yun⁹, F. Zetti¹², T. Zimmerman⁹, S. Zimmermann¹², S. Zucchell⁸

Abstract-- We describe the characteristics of silicon microstrip sensors fabricated by Hamamatsu Photonics for the CDF Run 2b silicon detector. A total of 953 sensors, including 117 sensors from prototyping, have been produced and tested for electrical and mechanical properties. Five sensors were irradiated with neutrons up to 1.4×10^{14} n/cm², as a part of the sensor quality assurance program. The electrical and mechanical characteristics are found to be superior in all aspects and fulfill our specifications. We comment on charge-up susceptibility of the sensors that employ <100> wafers.

I. INTRODUCTION

THE CDF collaboration has designed a new silicon tracker system [1] for Tevatron Collider Run 2b. The system is a six double-layer device located between 2.1 cm and 17 cm radius, consisting of about 2300 single sided silicon

microstrip sensors. The whole detector is divided into an inner layer (L0) with 144 axial sensors and five outer layers (L1 to L5) with 2160 sensors between axial (1512 sensors) and 1.2 degree stereo (648 sensors). In the following we report on the outer sensors results as the small fraction of the inner sensors are similar although smaller in size (78.5 mm \times 15 mm) and with a finer pitch (25 μ m with alternate readout strips). Details of the L0 design can be found in [2].

The outer layers are built out of compact stave structures [3]. Each stave consists of twelve silicon sensors. Layers 1 and 5 have axial sensors on both sides so the stave is double axial. Layers 2 to 4 have axial sensors on one side and stereo on the other side. The silicon sensors are glued to a carbon-fiber rohcacell sandwich structure with an internal bus cable and embedded cooling tubes. The cooling tube efficiently sinks the heat generated in the sensors after receiving radiation and in ASIC chips on hybrids. The hybrids are glued on the silicon sensors. Such staves are arranged in a 66 cm long cylindrical structure (a barrel) which surrounds the beamline (z direction) and are supported by CF bulkheads at each end. Fig. 1 shows an endview of a barrel. Two barrels (each containing 90 staves) cover the interaction region to $|\eta| < 2$ with a small gap between the barrels at $z=0$. Details of the stave design are given in [1, 3].

The sensors are p^+ microstrips on n -bulk with 512 AC-coupled readout strips. An un-read strip, called an intermediate strip, is located between readout strips in order to enhance the position resolution. The dimensions of axial (stereo) sensors are 40.6 (41.1) mm wide and 96.4 mm long so that two sensors can be taken from a 6" wafer. The sensors are fabricated by Hamamatsu Photonics (HPK). Table I summarizes the main specifications. We employed HPK standard 6" wafers of 320- μ m thickness and in <100> direction.

Manuscript received November 15, 2003. This work was supported in part by the Japanese Ministry of Education, Culture, Sports, Science and Technology under Grant in Aid for Scientific Research (KAKENHI) on Priority Areas, 13047101, and operated by Universities Research Association Inc. under Contract No.DE-AC02-76CH03000 with the United States Department of Energy..

¹University of Tsukuba, Tsukuba, Ibaraki 305-8571, Japan (K. Hara, e-mail: hara@px.tsukuba.ac.jp). ²Universita' di Padova and INFN-Padova, Italy. ³Johns Hopkins University, Baltimore, MD 21218F. ⁴Duke University, Durham, NC 27708. ⁵Purdue University, West Lafayette, IN 47907. ⁶University of Liverpool, Liverpool L69 7ZE England. ⁷University of New Mexico, Albuquerque, NM 87131. ⁸Universita' di Bologna and INFN-Bologna, Italy. ⁹Fermilab, Batavia, IL 60510. ¹⁰University of California, Davis, CA 95616. ¹¹University of Illinois at Urbana-Champaign, Urbana, IL 61801. ¹²Lawrence Berkeley Laboratory, Berkeley, CA 94720. ¹³Carnegie Mellon University, Pittsburgh, PA 15213. ¹⁴Universita' di California, Santa Barbara, CA 93160. ¹⁵Wayne State University, Detroit, MI 48202. ¹⁶Kyungpook National University, Daegu, 702-701 Korea. ¹⁷Academia Sinica, Taipei, Taiwan 11529, Republic of China. ¹⁸Pohjois-Savo Polytechnic (PSPT), Kuopio, Finland. ¹⁹Okayama University, Okayama 700-8530, Japan. ²⁰University of Helsinki and Helsinki Institute of Physics, Finland. ²¹Osaka City University, Osaka 558-8585, Japan.

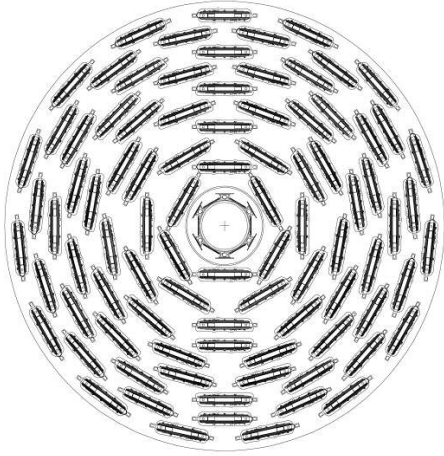


Fig. 1. Cross sectional view of the new silicon system, consisting of 90 staves in five layers, and a beam-pipe L0 layer (16 cm outer radius). Two sets are aligned in the beam direction covering 120 cm long region.

Table I. Main specifications of axial and stereo sensors

Specifications	Axial	Stereo
Wafer	<100>; 320±15μm thickness; <130μm warp	
Dimensions	40.55 x 96.392 mm	41.10 x 96.392 mm
Full depletion voltage	100 V < V _{dep} < 250 V	
Leakage current	< 2 μA at 20°C and at 500 V	
Number of strips	512 readout and 513 intermediate strips	
Strip widths	8 μm implant and 14 μm Al electrode	
Readout strip pitch (angle)	75 μm (0°)	80 μm (1.2°)
Coupling capacitor	capacitance > 120 pF; breakdown voltage >100 V	
Interstrip capacitance	< 1.2 pF/cm	
Poly silicon resistance	1.5±0.5 MΩ	
Defective strip fraction	< 1%	

We require that the sensors are radiation hard to 1.4×10^{14} 1-MeV equivalent neutrons per square centimeters, the fluence estimated to correspond to 30 fb^{-1} of Tevatron luminosity at the innermost layer. Specific requirements for radiation hardness of these sensors are the high voltage operation in excess of 500 V (this might be necessary after a large radiation dose) and the relatively high starting depletion voltage with a minimum value set at 100 V.

The system requires 1512 axial and 648 stereo sensors, and 953 have been delivered. First, we describe the electrical properties of the sensors. Five axial sensors were irradiated with neutrons up to $1.4 \times 10^{14} \text{ n/cm}^2$. The characteristics of these sensors are given. We observed some charge-up susceptibility and studied to understand its characteristics. Mechanical properties are also studied. Finally, we summarize the results.

II. ELECTRICAL PROPERTIES

A. General Quality Assurance (QA) Procedure

Hamamatsu Photonics performs intensive QA tests: I-V, C-V, AC-pad scan, and DC-pad scan. The AC-pad scan classifies defective strips as “AC Open” (the aluminum strip has a break), and “AC Short” (neighboring aluminum strips are shorted). The DC-pad scan reports “Open” (the implant strip has a break), “Short” (neighboring implant strips are shorted), “Leaky” (the individual strip current is large), and “Bad Isolation” (the interstrip resistance is small).

We have performed additional tests in order to verify the HPK test results and to evaluate the electrical characteristics in further detail. The tests are:

1. I-V curve: Total leakage current was measured up to 1000V bias at a step of 10V.
2. I-V curve stability: I-V curves were measured every 30 min at least for 10 times, typically 30 times. The bias voltage between the I-V measurements was set at 500 V.
3. C-V curve: Total capacitance was measured as a function of bias voltage. The curve was used to extract the full depletion voltage.
4. AC scan: Oxide coupling capacitance, equivalent series resistance (implant and bias resistance), and oxide punch-through at 100V were measured for each readout strip with an LCR meter.
5. DC scan: The leak current of individual strip was measured for sensors with large total leakage. The bias was set above the micro-discharge onset voltage.
6. Interstrip isolation: The interstrip resistance was measured with applying voltages (-1 to +1V) to the neighboring intermediate DC pads and measuring the current emerging from the readout DC pad.
7. Interstrip capacitance: The capacitance between the neighboring AC pads was measured with other strips floating to the ground.

We measured I-V and C-V characteristics for all the sensors. The AC scan and IV stability tests were performed on a sampling basis in order to verify the HPK probing results and to monitor the surface quality of the sensors. The rest of the tests were made less frequently. In particular they were used to diagnose sensors which deviated from the expected results.

B. I-V characteristics

The I-V curve is relatively easy to measure, yet providing overall view on the sensor quality. In Fig. 2 we show I-V curves of a typical subset of the sensors. The measured leakage current values were normalized at 20°C while the test bench temperature was in the range 26 to 30°C. The leakage current is quite small and most of the sensors do not show any significant micro-discharge up to 1000 V we measured. There are two sensors in this sample of 116 sensors showing micro-discharge

with the onset voltages of 800 and 900 V. For all 953 sensors the leakage currents at 500 and 950 V are shown in Fig. 3.

We set our leakage current requirement to be less than $2 \mu\text{A}$ at 500 V in order to insure that no single readout strip has a leakage current exceeding $\sim 1 \mu\text{A}$ as this would degrade the noise performance. All the sensors fulfilled this specification. In addition, 97% of the sensors showed leakage current below $0.5 \mu\text{A}$ even at 950 V. HPK has realized this superior performance by employing a single guard-ring structure with 1 mm distance between the scribed edge and the sensitive area.

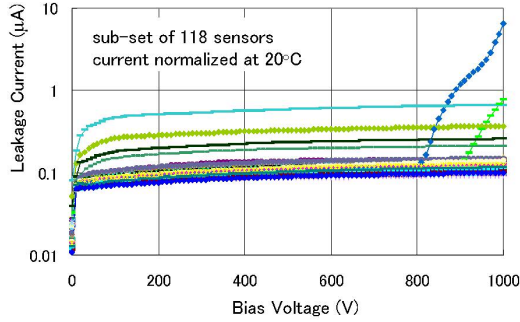


Fig. 2. Typical I-V curves (curves for 116 sensors are overlaid).

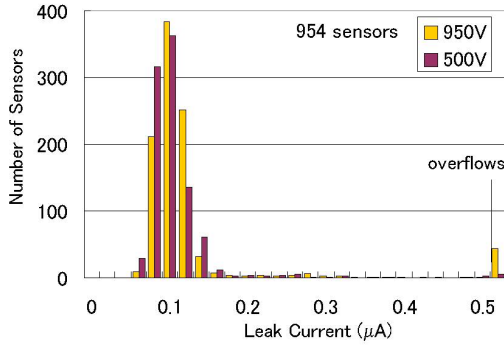


Fig. 3. Leakage currents at 500 and 950 V for all 954 sensors. The numbers exceeding $0.5 \mu\text{A}$ are given in extremely right bin

For the sensors that show micro-discharge, we have verified that the micro-discharge is caused at a single or a few strips by measuring the individual strip leakage (DC scan). It is possible to use these sensors by disconnecting those strips from the readout.

The leakage current of typical sensors increases to a $0.1 \mu\text{A}$ level in 30 V, this level being kept up to 1000 V. Such an I-V curve is not expected for sensors with full depletion voltages of about 100 V. We understand that the bulk current is quite small and the surface current is dominating in the low voltage region.

C. Stability of I-V curves

The I-V stability was measured for 42 sampled sensors. Between the I-V measurements, the sensors were biased at 500V for 30 min. The results can be categorized into four types, as shown in Fig. 4. For most of the sensors (35 sensors), the I-V curves were consistent and stable, as in Fig. 4(a). Two

sensors showed stability as shown in Fig. 4(b), where small micro-discharge developed above 900 V. We found four sensors that showed much significant micro-discharge as shown in Fig. 3(c). Two of them showed micro-discharge from the first measurement: the onset voltage increased gradually with time. The other two were good to 1000 V initially but the onset voltage of 600 V showed up within 1 hr. The onset voltage then increased with time, reaching 800 V or higher at the last measurement.

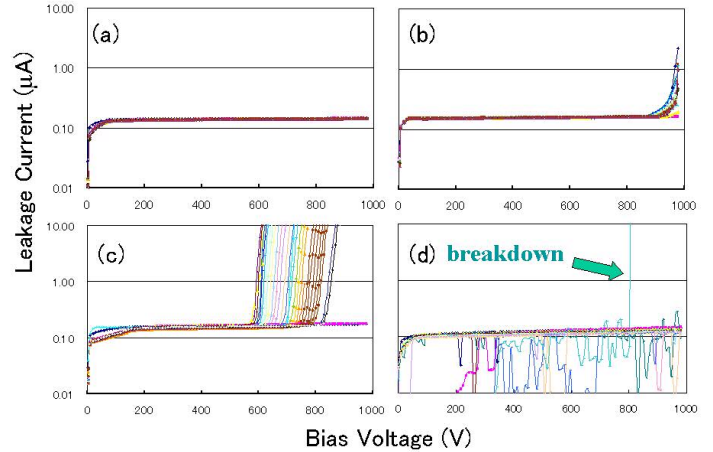


Fig. 4. Classification of I-V stability of 42 sensors. (a) Typical (35 sensors), (b) 2 sensors, (c) 4 sensors with significant micro-discharge, and (d) one sensor which showed breakdown at 800 V at 18th time.

An exceptional behavior was observed for one sensor. The I-V stability is shown in Fig. 4(d). The I-V, initially good to 1000 V, started to become chaotic after 8 hr and finally went to breakdown at 800V after 10 hr. We investigated the cause with an IR camera, and found a discharge hole on the bias-ring. Since we recognized no hint of discharge bridging to nearby structure, the discharge must have occurred towards the bulk substrate probably via some defect in the wafer. The sensor did not recover, indicating creation of permanent junction breakdown.

In summary, most sensors are good to 1000 V but some can create micro-discharge after a time scale of 1 hr. In either case, operation below 500 V should be safe.

D. Full Depletion Voltage

The C-V curves were measured for 908 sensors at an LCR frequency of 400 Hz. We extracted the full depletion voltage as the intercept of two straight lines in a $C^{-2} - V$ plot. The full depletion voltage distributed from 87 V and 165 V, as shown in Fig. 5.

Our depletion voltage specification of 100 V to 250 V is based on the resistivity range from 1.25 to 3.25 $\text{k}\Omega\text{cm}$, a wafer class employed by HPK. The minimum voltage of 100 V was not maintained: 7.7% of the sensors are out of specifications. This discrepancy is excused by HPK that the wafer resistivity is not uniform and applied resistivity sampling was not enough.

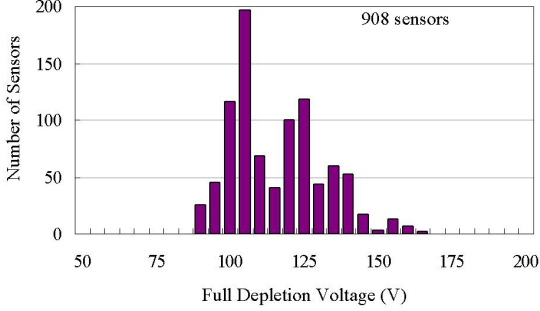


Fig. 5. Distribution of the full depletion voltages.

E. AC scan and Number of Defect Strips

The strip integrity was intensively evaluated by AC scan where the measurement was performed in two steps. Firstly, capacitance and series resistance were measured by probing between the AC pad and bias-ring setting the LCR meter at Cs-Rs mode and at 400 Hz. Secondly, 100 V pulse was applied across the oxide for 1 second and the leakage current through was measured. The capacitance represents the oxide coupling capacitance, and the resistance the sum of the bias resistance and implant electrode resistance. The implant resistance contributes approximately 0.3-0.5 M Ω .

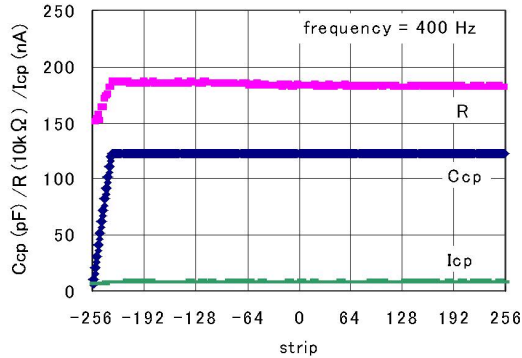


Fig. 6. AC scan result for a stereo sensor. The coupling capacitor C_{cp} increases with strip length and reaches about 120 pF. The series resistance R , starting from poly-silicon resistance of 1.5 M Ω , reaches about 1.8 M Ω .

AC scan was performed for 49 sensors. The coupling capacitors and resistors were found to be very uniform and defective strips can be easily identified: An example plot is given in Fig. 6. For the oxide leak current, the leakage through the CMOS relays that we used to isolate the LCR inputs from 100 V pulses contributes by a 10 nA level. This is larger than the leakage through genuine coupling capacitors, but is much smaller than the leakage through oxide punch-through of 10 μ A, which is defined by protection resistors in the system.

With HPK's AC scan, they evaluate various defects by injecting a step pulse into the bulk and measuring the signal emerging out from the AC pad, thus eliminating use of an LCR meter. One of the purposes of our AC scan is to compare the results.

The 49 sensors we selected have defects reported by HPK. Except for some leaky strips and bad isolation strips, we succeeded to identify all the other defects. Those unidentified defects can be ignored from the following reasons. Large leakage current tends to decrease with time, as described in Section II.C. Also, isolation degradation can be understood as non-permanent charge up, as is described in Section IV.

We created a couple of new damages associated with the probing system manipulation. Such damages are obvious by visual inspection. Apart from them, we have observed six new defects which were identified with a microscope as readout implant breaks.

Table II summarizes the number of defect strips measured by HPK. The percentages are given with respect to the total number of (readout or intermediate) strips of 488 thousands. Among these, the fraction of intermediate strip breaks is dominating. The readout implant breaks are substantially fewer, although we expect similar fractions if the breaks are created by dusts in the process. This apparent discrepancy is explained by the sensor layout and that HPK probing is barely sensitive to detect the readout implant opens. In our sensor layout, the poly-silicon resistors for readout strips are arranged at the probing side and those for intermediate strips at opposite side, the opposite side being completely passivated because the hybrid is glued on top. Because of this layout, the intermediate strip breaks are efficiently detected by probing DC pads and bias-ring, which is not the case for readout strips. In Table II we added six readout breaks with the fraction calculated for 49 sensors we measured. The fraction of readout implant breaks is comparable with that of intermediate implant breaks. We estimate the fraction of the readout strip defects to 0.04% adding the defects listed in the table.

Table II. Numbers and fractions of defect strips measured by HPK. The numbers in brackets are from our measurements.

Total number of strips	488k	
Readout implant break	2[+6]	[0.024%]
Interm. implant break	238	0.049%
Al electrode break	11	0.002%
Al electrode short	18	0.004%
Oxide punchthrough	17	0.003%
Poly-Si break	3	0.001%
Bad isolation	7	0.001%

F. Other Electrical Properties

1) Interstrip Resistance

The interstrip resistance was evaluated by measuring the increase/decrease in the readout strip leakage current when DC voltages ($\pm 1, \pm 0.5$ V) were applied to the two intermediate strips at neighbor. The four resistance values so obtained were averaged to represent the interstrip resistance. Three axial

sensors were measured. One sensor showed resistance of in the 50-200 G Ω range, and other two sensors showed 100-300 G Ω .

2) Interstrip Capacitance

The interstrip capacitance was evaluated by probing neighboring (readout) AC pads with other Al electrodes at floating and the detector bias at 200 V. The LCR frequency was set to 1 MHz. We have measured the interstrip capacitance of in total 9 axial and 2 stereo sensors. Among 5600 pairs of strips, only two pairs showed irregular values of 5% off the nominal value of 3.2 pF.

III. PROPERTIES OF IRRADIATED SENSORS

A. Neutron Irradiation

Radiation damage of silicon sensors has been studied intensively for the application to *e.g.* LHC experiments [4]. In order to verify that our sensors are radiation hard to the similar level, we irradiated 5 sensors with neutrons at MNRC Irradiation Facility at UC Davis. Three of the sensors received $1.4 \times 10^{14} \text{ cm}^{-2}$ 1-MeV neutron equivalent fluence and the other two $1.4 \times 10^{14} \text{ cm}^{-2}$ 1-MeV equivalent. The irradiation time was 69 min in total. The actual doses were evaluated by sulfur activation to 0.67×10^{14} and to $1.40 \times 10^{14} \text{ n/cm}^2$ with typical uncertainty of 10%.

Right after the irradiation the sensors were stored at -7°C . The sensor temperature was then increased for certain periods so that the sensors should almost complete the initial annealing and to have the full depletion voltage almost at the minimum.

B. Total Leakage Current and Full Depletion Voltage

Fig. 7 shows the I-V curves of the irradiated sensors. The current is normalized at 20°C . The sensors do not cause any micro-discharge up to 1 kV and show clear shoulders indicating that dominating is the leakage current through the bulk.

The measurement of full depletion voltage is strongly affected by high leakage current and therefore was performed in the environmental chamber at -25°C . The full depletion voltages derived from C^2 -V plots ranged from 128 to 130 V for the sensors irradiated to $1.4 \times 10^{14} \text{ n/cm}^2$, and about 50 V for the sensors irradiated to $0.7 \times 10^{14} \text{ n/cm}^2$. These values are consistent with previous measurements [4], which predict that the full depletion voltage be around 120 V and 40 V, respectively.

The damage constant α is expressed by $\alpha = \phi \Delta I / V$, where ϕ is the neutron fluence, ΔI the increase in the total leakage current measured at full depletion voltage, and V the volume of the sensor. Previous studies show that the leakage current of irradiated sensors decreases (anneals) with time approaching to an asymptotic value. Because of this feature and temperature dependence of the leakage current, α is calculated after the annealing is almost completed and at 20°C . Systematic study of the annealing phenomena is available such as from Rose Collaboration [4]. At room temperatures, the current decreases

substantially within a month, approaching to an asymptotic damage constant of $3 \times 10^{-17} \text{ A/cm}$.

Instead of evaluating the damage constant, we use our results to evaluate the neutron fluence. The evaluated neutron fluence is $1.1 \times 10^{14} \text{ n/cm}^2$ for nominal of $1.4 \times 10^{14} \text{ n/cm}^2$, and is $(0.33-0.64) \times 10^{14} \text{ n/cm}^2$ for nominal of $0.7 \times 10^{14} \text{ n/cm}^2$. The present results prefer somewhat smaller neutron fluence but are in reasonable agreement.

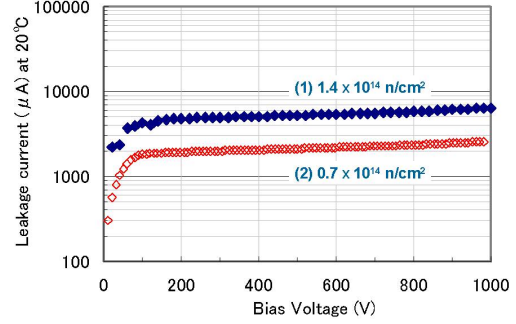


Fig. 7. I-V curves of irradiated sensors. The leakage current is normalized at 20°C . Sensor (1) was measured at 14°C and Sensor (2) at -15°C . Sensor (1) is not completely annealed while Sensor (2) should have completed the initial annealing.

C. Poly-silicon Resistance and Interstrip Resistance

The resistances of various sensor components are key properties to evaluate the radiation effect on silicon sensors. The oxide layer accumulates positive charges created due to radiation, which degrades such as poly-silicon resistance and interstrip resistance.

The poly-silicon resistance was measured and compared before and after irradiation. Fig. 8a shows the bias dependence measured for a particular strip. Although the resistance saturates below about 100V before irradiation, much larger bias voltage, about 350V, is required to reach the asymptotic value.

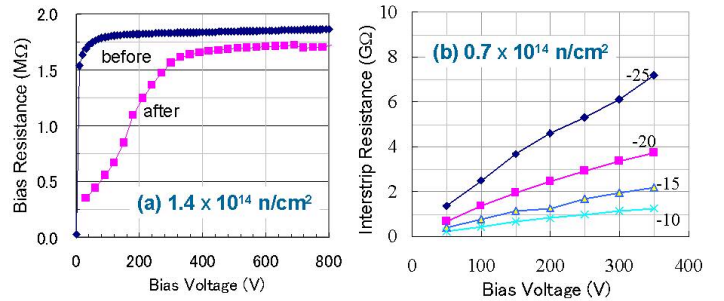


Fig. 8. (a) Poly-silicon resistance vs bias voltage and (b) interstrip resistance vs. bias voltage measured at various temperatures.

Fig. 8b shows the bias dependence of the interstrip resistance. The resistance is substantially degraded: it is greater than 50 G Ω before irradiation. In order to keep the resistance to be more than 1G Ω , a bias of 250V is required at -10°C .

Although the data are shown for a particular strip (pair), we found that the degradation is very uniform among the strips both for the poly-silicon resistance and interstrip resistance.

D. Interstrip Capacitance

Fig. 9 shows the bias dependence of the interstrip capacitance measured for a particular set of neighboring strips for two modules irradiated to 1.4×10^{14} n/cm². The two sensors were annealed similarly but the temperature was slightly different at measurement. The LCR frequency is 1 MHz. The shoulders around 130 V are consistent with the full depletion voltage. The interstrip capacitance decreases gradually with bias voltage, approaching to asymptotic values consistent with those of non-irradiated sensors. We notice, though, that the bias is substantially larger than the full depletion voltage to reach the asymptotic value.

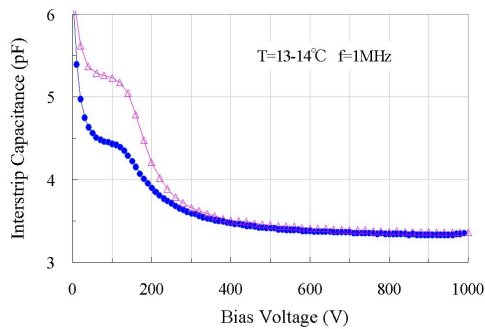


Fig. 9. Interstrip capacitance of irradiated sensors measured as a function of bias. The two sensors are measured at 13°C (filled circles) and at 14°C (open triangles).

E. Charge collection

The two sensors irradiated to 1.4×10^{14} n/cm² were used to construct a module where a readout hybrid was attached. This module was illuminated with Nd:YAG laser to investigate the charge collection. The laser wavelength 1064 nm corresponds to the energy slightly above the energy gap of silicon, hence the laser is absorbed almost uniformly along its trajectory, which simulates well the passage of charged particles.

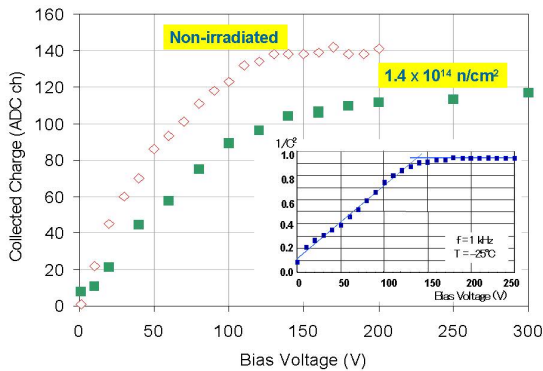


Fig. 10. Charge collection curve of irradiated sensors (filled squares) and of non-irradiated sensors (open diamonds). The inset is $C^{-2} - V$ curve of the irradiated sensor.

Fig. 10 shows the collected charge as a function of the bias voltage. Since the laser spot spreads over a few strips, ADC sum of neighboring strips is plotted. The same curve measured for a non-irradiated module is superimposed in the figure. We obtained somewhat smaller charges at saturation for the irradiated module, but the shapes are similar.

The voltage dependence of the charge collection is as expected from the C-V curve of the same sensor, which is shown in the inset in the figure.

IV. SENSOR SUSCEPTIBILITY OF CHARGE UP

In the early stage of testing, we often observed the sensor to show degraded performance in a region spreading over about 30 to 50 strips. The symptom is that the coupling capacitances are larger, the series (implant and poly-silicon) resistances are smaller, and interstrip resistances are smaller, which implies that the strip isolation is degraded in the region. After investigation it turned out that the vacuum tweezers used to pick up the sensor caused charge-up phenomenon. The phenomenon disappears if the sensor is placed back to the envelope provided by HPK.

The wafer orientation we employed is $\langle 100 \rangle$. Because positive charges trapped at the Si-SiO₂ interface and in the oxide layer are fewer for $\langle 100 \rangle$ than $\langle 111 \rangle$, they attract fewer electrons underneath the interface. Thus, external potentials can create easier a p⁺ layer, inversion layer, between the p⁺ strips, degrading the strip isolation. MOSFET devices usually use $\langle 100 \rangle$ wafers for this reason.

We observed that the charge-up phenomenon could remain at least for a week if the sensor surface is isolated. In practice, though, the wire-bonding to the amplifiers for example stabilize the Al electrode potentials and should eliminate the inversion layer. In order to verify this hypothesis, we created a charge-up sample and repeated the AC scan to monitor the recovery after three wires in the charge-up region were wire-bonded to the ground. The results are shown in Fig. 11.

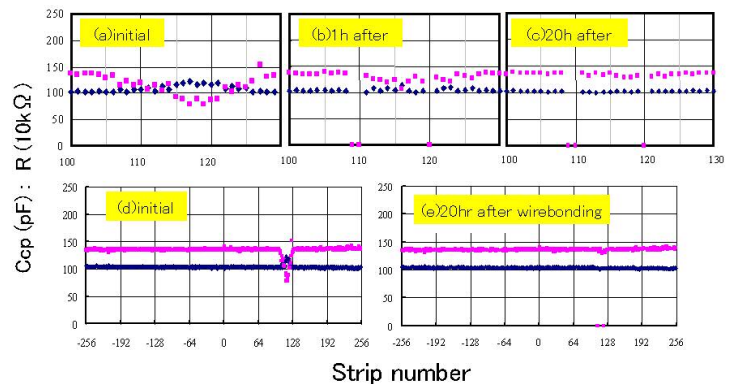


Fig. 11. AC scan results for charge-up study. (d) Initial distribution where strips 105 to 135 show irregular coupling capacitance (100 pF nominal) and series resistance (1.4 MΩ nominal). (a) Expanded plot of the charge-up region. (b) Enlarged plot 1 h after strips 109, 110 and 120 are wire-bonded. (c) Expanded and (e) entire distributions 20 h after. LCR frequency is 1 kHz.

The initial charge-up, as visible in Fig. 11(d), almost recovered 20 h after wire-bonding (Fig. 11(e)). The recovery seems to be somewhat slower at the mid-point between the wire-bonded strips; see the distribution 1 h after (Fig. 11(b)).

Although charge-up phenomena are therefore to disappear when the sensors are made into modules, we were able to diminish them by eliminating use of vacuum tweezers. Also we find that the charge-up susceptibility degrades with time: It became hard to charge-up the sensors 1 month after the delivery. Meanwhile the sensor probably accumulated positive charges in the oxide layer and became resistive against creation of inversion layer.

V. MECHANICAL PRECISIONS

Mechanical precisions of the prototype sensors were measured with a measuring microscope. The reproducibility is about 2 μm horizontally and 3 μm vertically.

A. Wafer thickness

The wafer thickness was measured for 78 sensors at the center of shorter sides. The sensors were placed vertically on the stage under the microscope. The central value was 320.4 μm a distribution as shown in Fig. 12. The precision quoted by HPK is 15 μm . The thickness difference at the two sides of the same sensor was at maximum 5 μm .

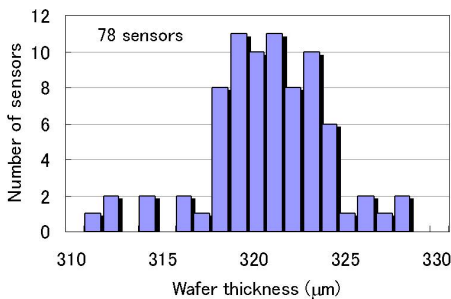


Fig. 12. Distribution of detector thickness.

B. Edge Cut Precision

The distance between the fiducial marks to the edge was measured at the four corners of 44 sampled sensors. The nominal distance is 330 μm . The distance distributed from 323 to 335 μm along the longer side and from 326 to 335 μm along the shorter side. The edge cut precision was better than 7 μm , while the quoted precision is 20 μm .

C. Sensor Planarity

The sensors tend to be bowed due to different thermal expansions between SiO_2 and Si: They are flat at high temperature when processed. The bow is more significant for single-sided sensors than for double-sided sensors.

The planarity was measured on 1 cm grids. Typical profile is given in Fig. 13, where the three corner data are used to define the reference plane and the deviations to it are plotted. The positive deviations mean that the sensor is bowed with the strips on the convex side. The profile is generally universal among the different sensors.

In order to increase the statistics, the height at the sensor center was measured with the microscope with respect to the heights at the fiducials at the four corners. The deviations distributed 80 to 100 μm for 11 axial sensors and 55 to 90 μm for 11 stereo sensors. The difference could be qualitatively explained by that the stereo sensors are wider than axial sensors. The twists, deviations of the 4th fiducial height which was not used to define the reference plane, distributed from -6 to 21 μm for the 22 samples.

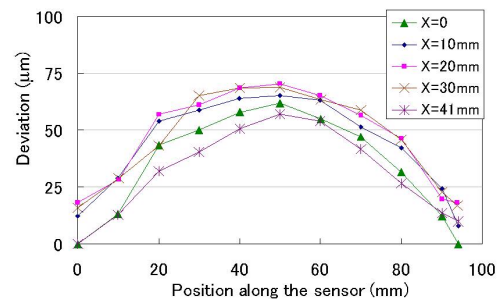


Fig. 13. Height profile of a stereo sensor measured on 1 cm grids.

VI. CONCLUSIONS

We evaluated the electrical and mechanical properties of microstrip sensors designed for the CDF Run2b silicon detector.

The leakage current is small (0.1 μA typically) and most sensors show no breakdown up to 1000V. The fraction of defective readout channels is estimated to 0.04%. The coupling capacitance, bias resistance and other electrical values are found to be uniform.

We have characterized various electrical parameters of the sensors irradiated with neutrons up to $1.4 \times 10^{14} \text{ cm}^{-2}$. The evolution of the full depletion voltage and increase of the leakage current are consistent with previously known values. Many parameters such as interstrip capacitance, interstrip resistance, and bias resistance are apparently degraded due to charges accumulated in oxide layer and type inversion. We observed that it requires a bias of 250-300V to reach the asymptotic values while the full depletion voltage is evaluated to be around 130 V.

The mechanical precisions, wafer width uniformity, edge cut precision and sensor bowing, were measured, all of which are found to be within our specifications.

VII. REFERENCES

- [1] M. Aoki et al. (CDF Collaboration), "CDF Run IIB Silicon Detector", submitted for Proceedings of 9th Pisa Meeting on Advanced Detectors,

- La Biodola, Isola d'Elba May 25, 2003; CDF Collaboration, "The CDF IIb Detector: Technical Design Report", FERMILAB-TM-2198 (Feb 2003).
- [2] P. Merkel (CDF Collaboration), "CDF Run IIb Silicon: The New Innermost Layer", submitted for IEEE NSS/MIC Conference, Portland, USA, October 19, 2003.
- [3] R.-S. Lu (CDF Collaboration), "Stave Design and Testing of SVXIIb of CDF at Fermilab", submitted for IEEE NSS/MIC Conference, Portland, USA, October 19, 2003; M.M. Weber (CDF Collaboration), "Electrical Performance and Dead-timeless Operation of "Staves" for the New CDF Silicon Detector", *ibid*; C. Cardoso (CDF Collaboration), "Polyimide and BeO Mini Portcard Performance", *ibid*.
- [4] ROSE Collaboration, see, for example, <http://cern.ch/rd48>.